

# FM2S: Self-Supervised Fluorescence Microscopy Denoising With Single Noisy Image

Jizhihui Liu, Qixun Teng, Junjun Jiang\*

Harbin Institute of Technology, Harbin 150001, China  
2023112090, 2023112559@stu.hit.edu.cn, jiangjunjun@hit.edu.cn

## Abstract

Fluorescence microscopy has significantly advanced biological research by visualizing detailed cellular structures and biological processes. However, such image denoising task often faces challenges due to difficulty in precisely modeling the inherent noise and acquiring clean images for training, which constrains most existing methods. In this paper, we propose an efficient self-supervised denoiser Fluorescence Micrograph to Self (FM2S), enabling a high-quality denoised result with a single noisy image. Our method introduces an adaptive global-local Noise Addition module for data augmentation, addressing generalization problems caused by discrepancies between synthetic and real-world noise. We then train a two-layer neural network to learn the mapping from the noise-added image to the filtered image, achieving a balance between noise removal and computational efficiency. Experimental results demonstrate that FM2S excels in various microscope types and noise levels in terms of denoising effects and time consumption, obtaining an average PSNR improvement of around 6 dB over the original noisy image in a few seconds. The code is available at <https://github.com/Danielement321/FM2S>.

## Introduction

Fluorescence microscopy has significantly advanced biological research in microstructures and biological processes by enabling visualization of cellular particles and molecules, where clear details are essential. However, noise corruption in images is usually inevitable, harshly degrading image quality. Meanwhile, the inherent noise distribution of fluorescence microscopy images (FMI) generally varies with different microscopes and in-camera signal processing pipelines, as well as other physical factors such as weak signal and diffraction limit (Zhou et al. 2020), which makes noise patterns more intricate than those in common images. Enhancing the laser power or exposure time might bring better noise-to-signal-ratio (SNR), however, it is accompanied by photobleaching and phototoxicity (Ma et al. 2024). Therefore, the denoising algorithm is crucial for fluorescence microscopy imaging.

For the FMI denoising task, the complexity of inherent noise in FMI hinders the effectiveness of conventional methods that require a noise prior, for example, using models

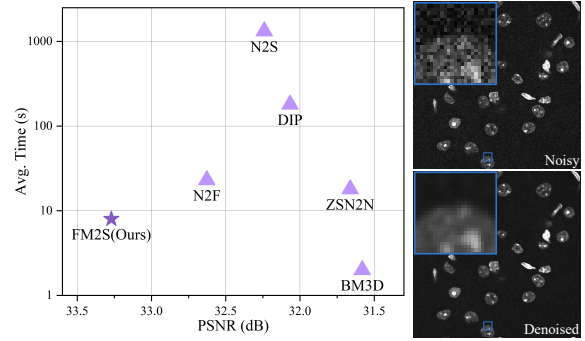


Figure 1: A demonstration of our method’s performance. The left figure shows denoising performance versus computational efficiency for dataset-free methods, and the right one displays our method for a real FMI.

such as signal-independent additive white Gaussian noise (Buades, Coll, and Morel 2010; Dabov et al. 2007) or spatially variant mixed Poisson-Gaussian noise (Meineli, Olivo-Marin, and Angelini 2018; Luisier, Blu, and Unser 2010). The inadequate performance is mainly because the model does not adequately match the actual noise distribution of FMI. Besides, the difficult acquisition of multiple noisy-clean paired images as training datasets limits the use of most supervised deep-learning methods, such as DnCNNs (Zhang et al. 2017) and FFDNets (Zhang, Zuo, and Zhang 2018). These drawbacks push the research of self-supervised methods, which train on the same image they denoise. Data augmentation is a key technique among these methods. Approaches like Noise2Fast (Lequyer et al. 2022) and Zero-Shot Noise2Noise (Mansour and Heckel 2023) generate training noisy pairs through downsampling, which may cause discrepancies between training and real noise. Another approach is mask scheme, as seen in Self2Self (Quan et al. 2020), where training pairs are generated by a Bernoulli sampler. However, this requires vast iterations and high computational costs. Additionally, methods like Noiser2Noise (Moran et al. 2020) add noise to generate training images but require a known noise distribution, limiting their practical applicability (Wang et al. 2022).

To tackle the above issues and limitations, we propose an efficient self-supervised denoiser FM2S that outperforms

\*Corresponding author

existing dataset-free methods in the FMI denoising task. Motivated by Noiser2Noise, our method adopts the approach of introducing added noise to train the denoiser. To address the out-of-distribution generalization problem, we design an adaptive global-local Noise Addition module for data augmentation, which mainly comprises Region-Wise Noise Addition and Overall Noise Addition to approximate synthetic noise to real noise. The module first adds mixed Poisson-Gaussian (MPG) noise based on regional pixel intensity, followed by global Poisson noise to the median-filtered image, enabling the network to learn the noise distribution accurately. To avoid overfitting and further enhance the network’s generalization ability, the module is executed multiple times to generate a set of noisy images for training. Moreover, we train the neural network (NN) directly with the complete image and confirm that a simple 2-layer network, with several thousand parameters, is sufficient for high-quality and computationally efficient denoising (Mansour and Heckel 2023). Our method demonstrates outstanding performance on FMI captured by various types of microscope and particularly excels in Wide-Field microscopes, which typically pose significant challenges for existing denoising techniques. Normally, our approach not only maintains high image quality but also preserves clear details. This capability highlights the robustness and adaptability of our method, making it ideal for FMI denoising across a range of microscopy. As shown in Fig. 1, compared with the recently leading self-supervised or dataset-free methods, our FM2S achieves near-optimal results, preserving clear structures and details across different sensors.

In summary, our contributions are as follows:

- This method is designed explicitly for denoising FMI. Compared to existing methods, it offers greater specificity and better preservation of image details.
- FM2S excels in processing speed and requires only several seconds to perform a satisfying denoising task, meeting the timely processing requirements of FMI.
- Our method achieves excellent results on FMI captured by different types of sensors. Notably, it performs exceptionally well on Wide-Filed sensors, which are generally challenging for existing methods.

## Related Works

**Supervised Denoisers** Supervised methods require extensive training data for denoising. DnCNN (Zhang et al. 2017) handles unknown noise levels trained by noisy-clean pairs as supervision. Advanced supervised denoisers were then proposed like Noise2Noise (Lehtinen et al. 2018) trained on only noisy images, which reduces the number of data collected. Most of such methods rely on a large network to learn multiscale features. However, training data still remain challenging to construct in practice, especially for FMI, because of the cost of acquisition, deformation, and contrast variations. Moreover, supervision with a specific prior often performs poorly when processing unknown noise patterns.

**Self-Supervised Denoisers** Self-supervised methods train on the same image they denoise. Noise2Noise inspired a

lot of later methods. Noisy-As-Clean (Xu et al. 2020) and Noiser2Noise (Moran et al. 2020) add noise for training denoisers, relying on a known noise distribution, which limits practical application. In contrast, Noise2Fast (Lequyer et al. 2022) and Zero-Shot Noise2Noise (Mansour and Heckel 2023) generate training noise pairs through downsampling. However, this process disrupts structural continuity and causes over-smooth by approximating neighbouring pixels. Noise2Void (Krull, Buchholz, and Jug 2019), Self2Self (Quan et al. 2020), and AP-BSN (Lee, Son, and Lee 2022) introduce mask scheme to denoise individual noisy images. However, the presence of blind spots in noisy images reduces denoising accuracy.

**Noise in Fluorescence Microscopy Image** The noise in FMI is more complex than a simple statistical distribution. Generally, the noise is sourced from the loss of photons and imperfect imaging system (Maji and Yahia 2019), *i.e.* quantum noise and thermal noise respectively. The former strongly correlates with pixel intensity, while the latter corrupts the whole image equally and is independent of pixel intensity (Mannam et al. 2022). The quantum and thermal noise can be separately explained as Poisson and Gaussian noise, and FMI noise can be seen as compound MPG noise (Zhang et al. 2019), which is neither additive nor multiplicative noise, limiting most denoising methods designed for fixed noise type.

## Proposed Method

Inspired by Noiser2Noise (Moran et al. 2020), our method adds adaptive noise to images and drives the network to learn the mapping from more-noise images to less-noise images. The pipeline is displayed in Fig. 2. Unlike methods that utilize downsampling or blind-spot network (Wang et al. 2022; Laine et al. 2019; Krull, Buchholz, and Jug 2019), which may change noise type or damage certain details of the image, our method trains a simple plain NN to learn the noise mapping with the entire image directly, ensuring consistency in training and inference, making sufficient retention of image information.

## Motivation

**Noiser2Noise** In Noiser2Noise, a noisy image is added with noise following a simple statistical distribution with a fixed intensity, which are respectively the target and input of NN. The noisy image and noisier image can be denoted as  $y_1 = x + n_1$  and  $y_2 = y_1 + n_2$ , where  $x$  denotes the image with no noise, and  $n_1, n_2$  denote noise that follows the same model. For additive zero-mean Gaussian noise, the basic idea includes estimating  $\mathbf{E}(y_1|y_2)$  by NN, and then obtaining  $\mathbf{E}(x|y_2)$  by  $2\mathbf{E}(y_1|y_2) = \mathbf{E}(x|y_2) + y_2$ , generating an estimate of  $x$ .

With some improvements, such as adjusting additive noise distribution  $n_2$ , Noiser2Noise outperforms methods like Noise2Void, DIP, and BM3D. However, in the original implementation of Noiser2Noise, the drawback is obvious for it requires an explicit noise model, and a different estimation should be constructed for the corresponding noise type. Moreover, for compound noise like MPG, the accurate

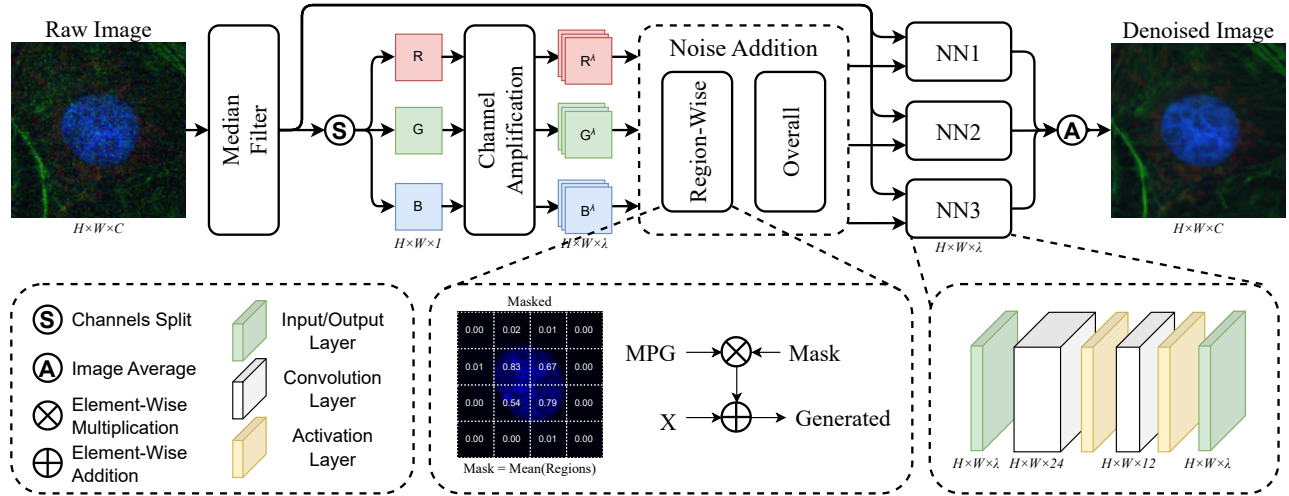


Figure 2: The whole pipeline of FM2S. The original image is first median-filtered to generate an image with relatively less noise, which will be used for Noise Addition and act as the training target for NNs. Noise Addition applies adaptive MPG to the filtered image and generates samples similar to real ones, where channel amplification is taken to enhance the generalization ability of NN. After training, the original noisy image is split and amplified, and the NNs will directly yield the denoised image.

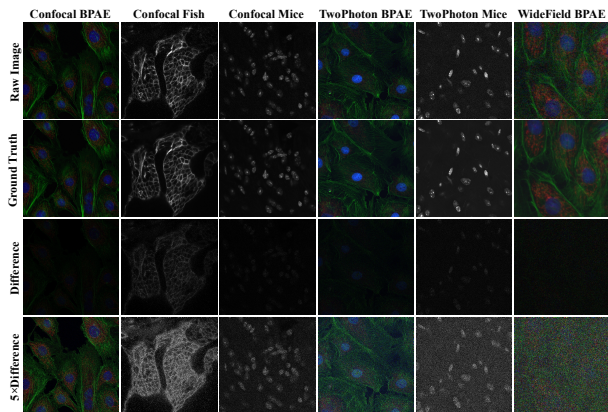


Figure 3: The difference between real noisy image and ground truth. The first and second rows are original noisy images and corresponding ground truth. The third row is the difference between the original image and ground truth, *i.e.*, noise. The fourth row is five times the difference and can be seen as the brightened noise for better visualization.

output can hardly be built by a simple math model, deteriorating the denoising performance for FMI.

In our method, we obtain the noisier image by adding adaptive MPG with the Noise Addition module, which simulates the real noise in FMI. Due to the non-linearity and complexity of noise, we change the training target and input to be the filtered image with less noise  $\hat{x}_i$  and augmented data  $y_i$ , *i.e.*, to train a network to predict  $\mathbf{E}(\hat{x}_i|y_i)$ . At the inference stage, the network will directly output denoised  $\mathbf{E}(\hat{x}|y)$  according to the mapping learned from training, where  $y$  denotes the original image and  $\hat{x}$  denotes denoised image.

**Noise Observation** Image denoising is defined as removing noise in the original noisy image, so it is crucial to have an insight into the noise itself. However, FMI noise is mainly a complex mixture of Poisson and Gaussian noise (Zhang et al. 2019), which makes it hard to build an accurate noise model or conduct quantitative analysis.

Despite the difficulties, we take a simple and intuitive approach to studying the noise. A noisy image  $y$  corrupted with latent ground truth  $x$  can be modeled as

$$y = \sigma(x) \quad (1)$$

where  $\sigma(\cdot)$  denotes the noise corruption. Suppose the ground truth  $x$  is given. In that case, the aim of denoising is to solve

$$\arg \min_{\theta} \|f_{\theta}(\sigma(x)) - x\|_F \quad (2)$$

where  $f_{\theta}$  denotes NN with parameter  $\theta$  and  $\|\cdot\|_F$  denotes Frobenius norm. However,  $x$  can not be known priorly in self-supervised denoising.

Fig. 3 shows the difference between noisy FMI and ground truth, which is the optimization target. It can be observed that the noise in brighter areas is more intense than that in the darker areas. The phenomenon seems contradictory to common images such as mobile phone images, where low light causes noise (Chen 2019), but has its root in the inherent weak signal of fluorescence. Zhang et al. point out that photons captured by microscope sensors are much fewer than in a common photograph, *i.e.*, the signal enhancement by more photons is less than the noise caused by the increment of photon discrete degree, which is also accompanied with more photons. As a result, the brighter areas show more noise because of uncertainty caused by photon detection.

## Preprocessing of The Noisy Image

**Median Filter** In FM2S, the median filter serves two key roles: input for Noise Addition and network training tar-

get. Directly adding synthetic noise to the original noisy image generates images much noisier than real ones, which is against the consistency rule of sample augmentation. To address this problem, we introduce median filter first to obtain an image with relatively less noise as the input of Noise Addition. In addition to Noise Addition, considering that the filtered image is less corrupted with noise, it also serves as the training target for NN, which is crucial to the whole pipeline.

The median filter shifts the optimization target from Eq. 2 to solve

$$\arg \min_{\theta} \|f_{\theta}(\hat{\sigma}(u)) - u\|_F \quad (3)$$

where  $u$  denotes the filtered noisy image  $y$  and  $\hat{\sigma}(\cdot)$  denotes simulated noise corruption, which is the Noise Addition module. In this way,  $u$  can be obtained by applying median filter on the noisy image, which can be achieved in practice. Changing either  $u$  in Eq. 3 will break the its consistency with Eq. 2, causing suboptimal performance.

**Channel Amplification** To further enhance the network’s generalization ability, we introduce Channel Amplification before the Noise Addition module, which increases the number of training samples with high parallel efficiency. This is done by first splitting the channels of the filtered input image and then repeating every channel for  $\lambda$  times. Given a filtered image  $I_{filtered} \in \mathbf{R}^{H \times W \times C}$ , the split process can be modeled as

$$I_{amp}(h, w, i_k) = I_{filtered}(h, w, k) \quad (4)$$

where  $i_k = 1, 2, \dots, \lambda$  and  $k = 1, 2, \dots, C$ .  $I_{amp}$  denotes the amplified image, and  $I_{filtered}$  denotes the filtered image. Among them,  $\lambda$  denotes the amplification factor.

### Noisy Sample Generation by Noise Addition

The purpose of the Noise Addition module is to generate noisy samples that feature noise distribution similar to the real ones, serving as data augmentation executed multiple times. For this aim, we design Region-Wise Noise Addition and Overall Noise Addition.

**Region-Wise Noise Addition** As the previous subsection mentioned, although the exact noise distribution ratio can not be examined (or fails to reach a satisfying performance for FMI (Chen, Zhu, and Ann Heng 2015)), a qualitative observation can be drawn that the MPG noise in brighter areas is more intense than the darker areas. To simulate the noise distribution, we design Region-Wise Noise Addition, which applies adaptive MPG noise to regions of the image based on regional pixel intensity.

In this step, a mask indicating the region intensity of MPG is first generated. Specifically, the mask  $M_{[k]}$  is the mean of pixel intensity, where  $k$  denotes the label of region framed by sliding window. Subsequently, the Poisson distribution factor  $\lambda_{p[k]}$  and Gaussian standard deviation  $\sigma_{g[k]}$  for  $k$ -th region is determined by corresponding mask  $M_{[k]}$

$$\sigma_{g[k]} = k_g \times M_{[k]} \quad (5)$$

$$\lambda_{p[k]} = \frac{k_p}{M_{[k]}} \quad (6)$$

where  $M_{[k]}$  denotes the  $k$ -th region of the whole image,  $k_g$  and  $k_p$  respectively denotes Gaussian mapping factor and Poisson mapping factor, which are hyperparameters optimized for specific microscopes. After obtaining the noise distribution factor for each region, adaptive MPG will be added to each region.

$$x_{i,j} = x_{i,j}^p + x_{i,j}^g \quad (7)$$

where  $x_{i,j}$  denotes  $(i, j)$  pixel with the addition of adaptive noise in  $k$ -th region,  $x_{i,j}^p$  denotes pixel with added Poisson noise, following  $\lambda_{p[k]} x_{i,j}^p \sim P(\lambda_{p[k]} x_{i,j})$ , and  $x_{i,j}^g$  denotes pixel with Gaussian noise, following  $x_{i,j}^g \sim N(0, \sigma_{g[k]}^2)$ .

**Overall Noise Addition** As Fig. 3 shows, noise still exists in darker areas. Mannam et al. points out that thermal noise caused by electronic components exists in the whole image, independent of the pixel intensity. Therefore, depending solely on Region-Wise is insufficient to simulate real noise to a certain extent. To address this problem, we take a simple approach of directly adding Poisson noise to the whole image, which proves necessary to the whole data augmentation process by ablation study. The process can be modeled as

$$x_{i,j} = x_{i,j}^p \quad (8)$$

where  $x_{i,j}$  denotes  $(i, j)$  pixel after Overall Noise Addition,  $x_{i,j}^p$  denotes pixel with Poisson noise, following  $\lambda_p x_{i,j}^p \sim P(\lambda_p x_{i,j})$ , where  $\lambda_p$  denotes the distribution factor for Poisson noise, which is optimized for specific microscopes.

### Network Architecture

For dataset-free image denoising, overfitting is more common because of the insufficient samples. Thus, larger networks may lead to worse results than smaller ones. Inspired by other dataset-free methods (Mansour and Heckel 2023), we design a compact network with much fewer parameters than a U-Net widely used in deep-learning-based image denoising algorithms. Discussion on different networks can be found in our supplementary material. As Fig. 2 displays, the network comprises two convolution layers with  $3 \times 3$  kernel size and padding to ensure the size of the image remains unchanged. Each convolution layer follows an activation layer of LeakyReLU. The input of the network is amplified image  $I_{in} \in \mathbf{R}^{H \times W \times \lambda}$  and the output is  $I_{out} \in \mathbf{R}^{H \times W \times \lambda}$ , which have the same size.

## Experiments

We test our method and several baselines with real FMI at different noise levels. Besides, experiments on some key hyperparameters and modules are conducted.

### Experimental Settings

**Dataset** Our experiments are completed with the Fluorescence Microscopy Denoising (FMD) dataset, which is specifically established to serve denoising tasks for FMI (Zhang et al. 2019). The dataset is constructed by three kinds of commercial microscopes: Confocal, Two-Photon, and Wide-Field, and has representative bio-samples. The authors employ image-averaging to obtain ground truth, which

Method	Confocal		Two-Photon		Wide-Field		Average	
	PSNR	SSIM	PSNR	SSIM	PSNR	SSIM	PSNR	SSIM
Noisy	29.1284	0.7100	26.3167	0.4781	25.2311	0.3674	27.2168	0.5471
Median Filter	33.4726	0.8682	31.5647	0.7693	28.3866	0.5626	31.5651	0.7588
BM3D	31.2783	0.8197	32.2018	0.8786	<b>31.2562</b>	<b>0.7599</b>	31.5806	<b>0.8244</b>
DIP	33.9367	0.9022	32.3547	0.8526	28.5662	0.6028	32.0668	0.8108
N2F	<b>35.6951</b>	<b>0.9359</b>	<b>33.8805</b>	<b>0.8974</b>	25.8443	0.3955	<b>32.6275</b>	0.7886
N2S	34.5141	<b>0.9240</b>	<b>33.5982</b>	<b>0.8914</b>	26.6401	0.4511	32.2403	0.7949
ZSN2N	34.2729	0.9098	32.7641	0.8689	25.8397	0.3979	31.6617	0.7682
FM2S	<b>34.9948</b>	0.9089	33.4639	0.8830	<b>30.1395</b>	<b>0.7066</b>	<b>33.2707</b>	<b>0.8497</b>

Table 1: The denoising performance of FM2S and baselines on the noisy images from the FMD official test set. The best results are in **bold**, and the second best are *italicized*.

is estimated by an average of 50 noisy raw images. In addition to ground truth, the dataset also provides noisy images at five different noise levels obtained by averaging 1, 2, 4, 8, and 16 noisy raw images.

**Baselines** We compare FM2S with other dataset-free denoising methods, including traditional and deep-learning-based methods.

For traditional methods, we compare with BM3D (Dabov et al. 2007) and median filter. BM3D requires a prior standard deviation for the Gaussian noise, and with the aim of denoising with a single image, the whole pipeline is to first use Median Absolute Deviation (MAD) (Donoho and Johnstone 1992) to estimate the noise standard deviation  $\sigma$ , and then apply BM3D with  $\sigma$  to denoise. Median filter is another traditional denoising algorithm, as well as it is used in our FM2S to obtain a target with relatively less noise. The window size is 3 in this implementation.

Regarding deep-learning-based methods, we compare the proposed method with Deep Image Prior (DIP) (Ulyanov, Vedaldi, and Lempitsky 2018), Noise2Fast (N2F) (Lequyer et al. 2022), Noise2Self (N2S) (Batson and Royer 2019) and Zero-Shot Noise2Noise (ZSN2N) (Mansour and Heckel 2023). DIP’s performance is sensitive to the number of iterations, and we set the iterations to be 3000, the same as the original setting. For other methods, schemes like downsampling are utilized in N2F and ZSN2N, managing to denoise without substantial training data. The methods all follow their original implementations.

**Implementation Details** In our implementation, we utilize the Adam optimizer (Kingma and Ba 2014) to update the network, with an initial learning rate of 0.001 and  $\beta_1 = 0.9$ ,  $\beta_2 = 0.999$ . The learning rate is scaled by 0.25 every 1500 epoch, and pixel-wise  $L_2$  loss is used. For Region-Wise Noise Addition, the mapping factor for Gaussian and Poisson noise are  $k_{gau} = 200$ ,  $k_{poi} = 30$ . As for Overall Noise Addition, the Poisson noise distribution factor  $\lambda_p = 60$ . Because the test set given by dataset authors is in single-channel grayscale, all the methods are evaluated with single-channel images. All the experiments are completed on a platform with one Nvidia RTX 4070 SUPER GPU and Intel Core 13400F CPU.

## Main Results

### Evaluation on Real Fluorescence Microscopy Images

We evaluate our method’s denoising performance on the test set given by FMD dataset authors Zhang et al. The images are all original noisy images, which is what bio-researchers deal with. In this implementation, the Sample Size, Epoch Per Image (EPI), and Amplification Factor are 25, 150, and 2, respectively. We also evaluate other zero-shot methods with the same data, with results shown in Table 1.

The results indicate that FM2S has the best performance on average, denoting extraordinary denoising ability for general FMI. We notice that for Wide-Field micrographs, despite slightly falling short of BM3D, FM2S outperforms the other methods to a certain extent. It is plausibly because the noise in Wide-Field microscopes is mostly Gaussian noise (Zhang et al. 2019), which is exactly what BM3D deals well with. While for Confocal and Two-Photon microscopes, where Poisson noise dominates, BM3D’s performance drops sharply. Besides, the noise is spatially correlated in Wide-Field images (Lin et al. 2023), causing decreased results for most methods designed for additive noise.

For Confocal and Two-Photon images, despite FM2S not achieving the best results, it ranks second and third among all the methods. The reason may be that the complex MPG in these images requires a larger network to learn, which is discussed in our supplementary material, while in this implementation, FM2S only has 3.2k parameters to ensure a balance between performance and efficiency. Considering that it only takes a few seconds to denoise an image, the results are satisfying, especially for large-scale data.

Moreover, FM2S significantly outperforms the median filter, which serves as the training target for NN, indicating that the network effectively learns the mapping from intense noise to weak noise and successfully applies this mapping to the raw image for improved denoising.

One demo of our method and baselines can be found in Fig. 4. FM2S removes most of the noise and preserves fine details. In this demo, our method’s PSNR and SSIM are similar to those of N2F and N2S. However, due to the downsampling and mask scheme employed in the two methods, FM2S shows higher image contrast, which can be observed in the green ROI.

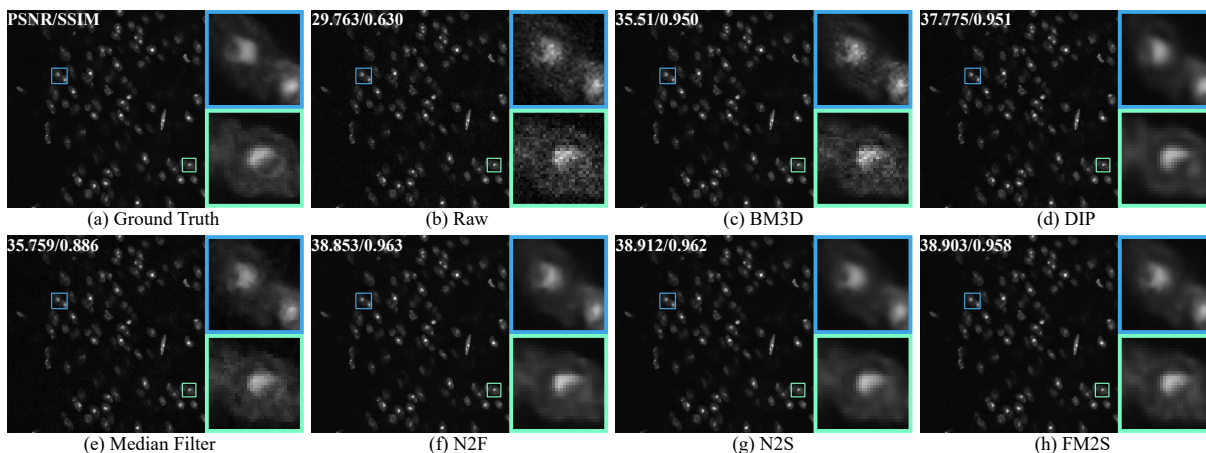


Figure 4: A fluorescent micrograph for mouse brain tissue captured by Confocal microscope from FMD dataset, with PSNR(dB) and SSIM labeled on the top left corner.

Noise Level	Noisy	Median_F	BM3D	DIP	N2F	ZSN2N	FM2S	FM2S*
avg1	27.2168	31.5651	31.5806	32.0668	32.6275	31.6617	<b>33.2551</b>	<b>33.2814</b>
avg2	30.0777	33.2857	33.7397	33.3743	32.9766	33.2493	<b>34.4692</b>	<b>34.6021</b>
avg4	32.8606	35.1610	<b>36.0067</b>	34.8535	35.8507	35.3315	35.3347	<b>36.5660</b>
avg8	36.0268	36.6037	<b>37.7441</b>	36.0500	37.7399	37.7049	35.9711	<b>38.2366</b>
avg16	39.7026	38.2667	39.3696	36.8968	40.0987	<b>40.8523</b>	36.5146	<b>40.7475</b>

Table 2: The PSNR(dB) for FM2S and baselines on images with different noise level. FM2S denotes our original implementation, while FM2S\* denotes the implementation manually fine-tuned for specific noise level. ‘avg1’ denotes original noisy images from the test set, marking the highest noise level, as well as ‘avgN’ denotes the images obtained by averaging  $N$  noisy images, thus lower noise level for higher  $N$ . The best results are in **bold**, and the second best are *italicized*.

**Evaluation on Different Noise Level** We examine our method’s denoising performance with FMI at different levels. The images are obtained by averaging noisy images and still follow real noise distribution.

In Table 2, we present the denoising effects of FM2S and other methods on FMI with varying noise levels. The results indicate that for images with high noise levels, FM2S outperforms other baselines significantly, which is exactly what bio-researchers need in practice. However, a performance drop in images with lower noise levels is observed. One possible reason for the drop is that in Noise Addition, noise distribution factors are optimized for original noisy images, which are corrupted by intense noise. This can be solved by fine-tuning the noise distribution factor for different denoising tasks, and detailed fine-tuning process can be found in the supplementary material.

**Computational Efficiency** In addition to denoising performance, we further evaluate the network size and resource consumption of FM2S. All experiments are carried out with a grayscale 512×512 image on the same platform. In this implementation, all the hyperparameters are the same as the one from the previous section. The deep-learning-based methods are executed on a GPU, while traditional methods do not rely on a GPU, they are implemented through the CPU.

As Table 3 displays, FM2S has the fewest parameters and FLOPs among all the deep-learning-based methods, bringing the least memory consumption and fastest speed. Benefiting from the compact network structure, FM2S can even be implemented on a CPU in an acceptable time of 3 minutes on the same platform. A conclusion can be drawn that our method features outstanding computational efficiency.

### Influences of The Hyperparameters

Intuitively, the performance of FM2S relies on the number of noisy samples (Sample Size) and the learning epoch per image (EPI). Determining an appropriate set of the two key hyperparameters is essential for balancing denoising performance and computational efficiency. We randomly choose images from the FMD dataset except the test set for this part. All experiments are repeated five times, and the final data is averaged to avoid accidental errors.

As Fig. 5 suggests, our method’s denoising performance positively correlates with Sample Size and EPI, which agrees with intuition. Unlike DIP, whose performance drops after a particular iteration number (Quan et al. 2020), FM2S displays stability over iterations, *i.e.*, performance remains relatively stable with the increase of iterations, which brings less manual intervention. Therefore, a saturation point can be observed for Sample Size and EPI, after which the increment of denoising performance is much slower than com-

Comparison	BM3D	Median Filter	DIP	N2F	N2S	ZSN2N	FM2S
Parameter Size	-	-	2.2M	259.2k	223.1k	22.2k	3.2k
FLOPs	-	-	155.6G	67.95G	58.6G	5.85G	0.86G
Memory	-	-	2317MB	513MB	1281MB	147MB	50MB
Time	2 sec.	0.2 sec.	3 min.	23 sec.	22 min.	18 sec.	8 sec.

Table 3: Computation consumption for FM2S and baselines. We display trainable network parameter size (Parameter Size), floating-point operations (FLOPs), memory consumption (Memory), and time consumption (Time) for each method. For the traditional methods without deep learning, we only display the time consumption.

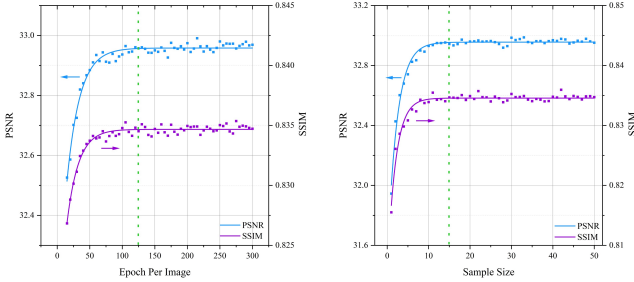


Figure 5: Denoising effect versus Sample Size and Epoch Per Image. The blue line denotes PSNR(dB) and the purple line denotes SSIM. The green dashed line denotes the saturation point.

putational consumption. We choose 25 and 150 as the best Sample Size and EPI, which ensures a satisfying denoising effect and computational efficiency.

## Ablation Studies

**Noise Addition Components** Noise Addition comprises Region-Wise Noise Addition and Overall Noise Addition, with the median-filtered image as input, and the output is a set of noisy samples for training. The ablation study for the Region-Wise strategy is done by removing the chunk identification and replacing it with the whole image, *i.e.*, to compute the mean of the entire image instead of the regions to get the synthetic noise factor. For the Overall strategy, we remove the corresponding step directly. Table 4 indicates that Region-Wise and Overall strategies are necessary for a better sample generation. Besides, the filtered image is more ideal for Noise Addition than the original image because the filtered image with additive noise is more similar to the original image than the original image itself with additive noise.

**Median Filter** The Median Filter generates image  $u$  in Eq 3, which is used for training target and Noise Addition. To confirm the necessity of Median Filter, we ablated it for the two steps respectively. For Noise Addition, we input the original noisy image into the Noise Addition module, and for Training Target, we use the raw image instead of the filtered one.

**Channel Amplification** We investigate the function of channel amplification present them in Fig. 4. In this implementation, the amplification factor  $\lambda$  is 2, and more detailed

Ablation(w/o)	Confocal	Two-Photon	Wide-Field
Filter	36.5152	33.3340	29.9316
Region-Wise	36.1888	33.8902	30.1144
Overall	36.6980	33.8680	29.8661
Channel Amp.	36.7038	33.8811	31.3763
Original	37.0743	34.1420	30.0955

Table 4: Ablation study of components in FM2S. The first row displays three types of microscopes, and the first column is the ablated component. 'Original' denotes the original implementation with full components, while 'w/o' denotes without the corresponding one. The results are shown in PSNR(dB).

	w/ NA	w/o NA
w/ TT	33.3821	32.9230
w/o TT	32.1758	31.3328

Table 5: Ablation of Median Filter for Noise Addition and Training Target. The results are shown in PSNR(dB).

results can be found in the supplementary material. The results show that the NN without channel amplification fails to remove most of the noise due to the inability to generalize. Since the best amplification factor varies with microscope types, and the type of microscope can be known explicitly in practical use, the factor can be set accordingly, bringing better performance than experiment results.

## Conclusion

In this paper, we propose a self-supervised denoising method, FM2S, for fluorescence microscopy images, with no need for a noise model or extra data than a single noisy image to perform an efficient denoising task. The method features an adaptive global-local Noise Addition module and takes full advantage of the inherent attributes of fluorescence microscopy noise, achieving extraordinary performance for fluorescence microscopy images. With a simple 2-layer network, FM2S achieves an excellent balance between computational efficiency and denoising performance, surpassing most of the current dataset-free methods, making it ideal for practical biology study.

## References

- Batson, J.; and Royer, L. 2019. Noise2self: Blind denoising by self-supervision. In *International Conference on Machine Learning*, 524–533. PMLR.
- Buades, A.; Coll, B.; and Morel, J.-M. 2010. Image denoising methods. A new nonlocal principle. *SIAM review*, 52(1): 113–147.
- Chen, G.; Zhu, F.; and Ann Heng, P. 2015. An efficient statistical method for image noise level estimation. In *Proceedings of the IEEE International Conference on Computer Vision*, 477–485.
- Chen, G. Y. 2019. An experimental study for the effects of noise on face recognition algorithms under varying illumination. *Multimedia Tools and Applications*, 78: 26615–26631.
- Dabov, K.; Foi, A.; Katkovnik, V.; and Egiazarian, K. 2007. Image denoising by sparse 3-D transform-domain collaborative filtering. *IEEE Transactions on image processing*, 16(8): 2080–2095.
- Donoho, D.; and Johnstone, I. 1992. Ideal spatial adaptation via wavelet shrinkage. *Biometrika*. To appear. Technical report, Also Tech. Report, Department of Statistics, Stanford University.
- Kingma, D. P.; and Ba, J. 2014. Adam: A method for stochastic optimization. *arXiv preprint arXiv:1412.6980*.
- Krull, A.; Buchholz, T.-O.; and Jug, F. 2019. Noise2void-learning denoising from single noisy images. In *Proceedings of the IEEE/CVF conference on computer vision and pattern recognition*, 2129–2137.
- Laine, S.; Karras, T.; Lehtinen, J.; and Aila, T. 2019. High-quality self-supervised deep image denoising. *Advances in Neural Information Processing Systems*, 32.
- Lee, W.; Son, S.; and Lee, K. M. 2022. Ap-bsn: Self-supervised denoising for real-world images via asymmetric pd and blind-spot network. In *Proceedings of the IEEE/CVF Conference on Computer Vision and Pattern Recognition*, 17725–17734.
- Lehtinen, J.; Munkberg, J.; Hasselgren, J.; Laine, S.; Karras, T.; Aittala, M.; and Aila, T. 2018. Noise2Noise: Learning image restoration without clean data. *arXiv preprint arXiv:1803.04189*.
- Lequyer, J.; Philip, R.; Sharma, A.; Hsu, W.-H.; and Pelletier, L. 2022. A fast blind zero-shot denoiser. *Nature Machine Intelligence*, 4(11): 953–963.
- Lin, H.; Zhuang, Y.; Ding, X.; Zeng, D.; Huang, Y.; Tu, X.; and Paisley, J. 2023. Self-supervised image denoising using implicit deep denoiser prior. In *Proceedings of the AAAI Conference on Artificial Intelligence*, volume 37, 1586–1594.
- Luisier, F.; Blu, T.; and Unser, M. 2010. Image denoising in mixed Poisson–Gaussian noise. *IEEE Transactions on image processing*, 20(3): 696–708.
- Ma, C.; Tan, W.; He, R.; and Yan, B. 2024. Pre-training a foundation model for generalizable fluorescence microscopy-based image restoration. *Nature Methods*, 1–10.
- Maji, S. K.; and Yahia, H. 2019. A feature based reconstruction model for fluorescence microscopy image denoising. *Scientific Reports*, 9(1): 7725.
- Mannam, V.; Zhang, Y.; Zhu, Y.; Nichols, E.; Wang, Q.; Sundaresan, V.; Zhang, S.; Smith, C.; Bohn, P. W.; and Howard, S. S. 2022. Real-time image denoising of mixed Poisson–Gaussian noise in fluorescence microscopy images using ImageJ. *Optica*, 9(4): 335–345.
- Mansour, Y.; and Heckel, R. 2023. Zero-shot noise2noise: Efficient image denoising without any data. In *Proceedings of the IEEE/CVF Conference on Computer Vision and Pattern Recognition*, 14018–14027.
- Meinzel, W.; Olivo-Marin, J.-C.; and Angelini, E. D. 2018. Denoising of microscopy images: a review of the state-of-the-art, and a new sparsity-based method. *IEEE Transactions on Image Processing*, 27(8): 3842–3856.
- Moran, N.; Schmidt, D.; Zhong, Y.; and Coady, P. 2020. Noisier2Noise: Learning to Denoise From Unpaired Noisy Data. In *Proceedings of the IEEE/CVF Conference on Computer Vision and Pattern Recognition (CVPR)*.
- Quan, Y.; Chen, M.; Pang, T.; and Ji, H. 2020. Self2self with dropout: Learning self-supervised denoising from single image. In *Proceedings of the IEEE/CVF conference on computer vision and pattern recognition*, 1890–1898.
- Ulyanov, D.; Vedaldi, A.; and Lempitsky, V. 2018. Deep image prior. In *Proceedings of the IEEE conference on computer vision and pattern recognition*, 9446–9454.
- Wang, Z.; Liu, J.; Li, G.; and Han, H. 2022. Blind2unblind: Self-supervised image denoising with visible blind spots. In *Proceedings of the IEEE/CVF conference on computer vision and pattern recognition*, 2027–2036.
- Xu, J.; Huang, Y.; Cheng, M.-M.; Liu, L.; Zhu, F.; Xu, Z.; and Shao, L. 2020. Noisy-as-clean: Learning self-supervised denoising from corrupted image. *IEEE Transactions on Image Processing*, 29: 9316–9329.
- Zhang, K.; Zuo, W.; Chen, Y.; Meng, D.; and Zhang, L. 2017. Beyond a gaussian denoiser: Residual learning of deep cnn for image denoising. *IEEE transactions on image processing*, 26(7): 3142–3155.
- Zhang, K.; Zuo, W.; and Zhang, L. 2018. FFDNet: Toward a fast and flexible solution for CNN-based image denoising. *IEEE Transactions on Image Processing*, 27(9): 4608–4622.
- Zhang, Y.; Zhu, Y.; Nichols, E.; Wang, Q.; Zhang, S.; Smith, C.; and Howard, S. 2019. A poisson-gaussian denoising dataset with real fluorescence microscopy images. In *Proceedings of the IEEE/CVF Conference on Computer Vision and Pattern Recognition*, 11710–11718.
- Zhou, R.; El Helou, M.; Sage, D.; Laroche, T.; Seitz, A.; and Süsstrunk, S. 2020. W2S: microscopy data with joint denoising and super-resolution for widefield to SIM mapping. In *Computer Vision–ECCV 2020 Workshops: Glasgow, UK, August 23–28, 2020, Proceedings, Part I 16*, 474–491. Springer.